Efficacy of Transcranial Magnetic Stimulation Targets for Depression Is Related to Intrinsic Functional Connectivity with the Subgenual Cingulate

Supplemental Information

Supplementary Methods

Subjects and Data Collection

Two datasets were used in the present analysis. The first consisted of 98 healthy right-handed subjects (48 male, ages 22 ± 3.2 years (mean ± SD)) collected in Boston, MA and was a subset of subjects previously used in an analysis of resting state functional connectivity (1). Experiments were conducted with the written consent of each subject and approved by the Partners' Institutional Review Board. Imaging was performed on a 3 T Siemens whole body MRI System with a phased array head coil. Each subject completed two 6.2 min long (124 frames) resting state functional magnetic resonance imaging (fMRI) scans (TR = 3000 ms, TE = 30 ms, FA = 85°, 3 x 3 x 3 mm voxels, FOV = 216, 47 axial slices with interleaved acquisition and no gap). During scanning, participants were instructed to keep their eyes open and remain still. All subjects were originally enrolled in an fMRI study on cognitive tasks; the resting state data used in this study was collected at the beginning of each subject's scan before any tasks were performed. Structural data included a high-resolution multi-echo T1-weighted magnetization-prepared gradient-echo image (TR = 2200 ms, TI = 1100 ms, TE = 1.54 ms for image 1 to 7.01 ms for image 4, FA = 7°, 1.2 x 1.2 x 1.2 mm voxels, FOV = 230) (2).

The second dataset consisted of 13 subjects with major depressive disorder (MDD; 3 male, mean age 40.2 years, mean Hamilton Depression Rating Scale (HAM-D) 23.8) and eleven healthy control subjects (5 male, mean age 29 years, mean HAM-D 0.4) collected in Palo Alto, CA. Data on 14 subjects with depression were originally collected, however one patient was excluded based on structural abnormalities on their MRI scan. Depressed subjects aged 18 – 65 years meeting DSM-IV criteria for major depression and a Hamilton Depression Rating Scale score > 18 were recruited utilizing online advertisements, radio advertisements and fliers posted in the community. Healthy controls not meeting criteria for MDD were subject to identical inclusion and exclusion requirements. All subjects underwent screening with the Structured Clinical Interview for DSM Disorders (SCID) by a trained psychologist. Subjects were excluded

if they had a history of significant head trauma, active abuse of alcohol or illegal substances, bipolar affective disorder, any psychotic disorder, obsessive-compulsive disorder, or any significant neurologic history (i.e. seizure, stroke, multiple sclerosis). Subjects had to be right-handed and could not have taken any psychotropic medication within two weeks of study enrollment. Depression severity was measured using the 21-item Hamilton Depression Rating Scale, Beck Depression Inventory, and the Montgomery Asberg Depression Rating Scale. The Stanford University Medical Center Institutional Review Board (IRB) approved the study, and all subjects signed an IRB approved informed consent. Imaging was performed at the Richard M. Lucas Center for Imaging at Stanford University on a 3-T General Electric Signa scanner using a standard whole-head coil. Each subject completed one 10 minute long (300 frames) resting state fMRI scan using a T2* weighted gradient echo spiral in/out pulse sequence (TR = 2000 ms, TE = 30 ms, FA = 80°, 3.4 x 3.4 x 4.5 mm voxels, 31 axial slices with interleaved acquisition, 4 mm thickness, and 0.5 mm gap). Patients were instructed to "lie still with your eyes closed, try not to think of any one thing in particular and try not to fall asleep." Structural data included a high-resolution T1-weighted spoiled gradient recalled 3-D MRI sequence (TR = 40 ms, minimum TE, FA = 11°, 0.86 x 0.86 x 1.2 mm voxels, 128 axial slices with interleaved acquisition).

A Priori Defined Regions of Interest

Several regions of interest (ROI) were defined a priori for use in the present analysis including one ROI in the subgenual cingulate cortex (Figure S1, Figure 5A) and multiple ROIs in the left dorsal lateral prefrontal cortex (DLPFC) (Figure 1, Figure 2). To construct an ROI in the subgenual cingulate cortex, we first identified coordinates from prior studies where a reduction in subgenual activity was associated with antidepressant response across a wide range of treatment modalities (3-9) (Table 1).

This is not intended to be an exhaustive list, but to sample the literature across a range of therapeutic interventions. We converted the reported subgenual coordinates (generally in Talairach space) into Montreal Neurological Institute (MNI) space using tal2mni (http://imaging.mrc-cbu.cam. ac.uk/imaging/MniTalairach). For the purposes of the current study, "Talairach" refers to the atlas coordinate space as defined by Talairach and Tournoux in 1988 (10). After conversion to MNI space, coordinates were averaged across all seven studies. We created a single 10 mm sphere centered on these coordinates (6, 16, -10) and masked this

ROI to exclude voxels not sampled in any of our 98 subjects or voxels falling outside of the cerebral cortex using the Harvard/Oxford cortical regions template available in FSL.

To construct left DLPFC regions of interest, we identified coordinates from a variety of studies of left DLPFC transcranial magnetic stimulation (TMS) (Table 2). Some studies focused on anatomical targeting (11-14), some on the physiological effect of TMS in normal subjects (15, 16), and some on anatomically defining Brodmann areas in the DLPFC (17) that have been suggested as optimal TMS stimulation sites (18).

For studies reporting Talairach coordinates, these were transformed into MNI space using tal2mni. For those studies reporting MNI coordinates (13) these were converted to Talairach coordinates using mni2tal (http://imaging.mrc-cbu.cam. ac.uk/imaging/MniTalairach). The coordinates for the Fitzgerald 2009 site were reported in Talairach coordinates in the initial publication (11), but MNI coordinates in a later publication by the same group (13). These later MNI coordinates (-46, 45, 38) are close but not identical to those obtained via tal2mni (-45, 45, 40), so we chose to use the previously published values (13). Since multiple studies reported average coordinates resulting from the 5 cm targeting method (12, 14), these coordinates were averaged to create one set of coordinates best representing the standard 5 cm target site. To generate coordinates for Brodmann regions (BA9 and 46) the average y and z Talairach coordinates were taken from Rajkowska and Goldman-Rakic 1995 (17). However this paper did not report x coordinates so this was determined from the coordinate in Talairach space on the cortical surface constrained by the y and z coordinates (10). This complete set of Talairach coordinates was then transformed into MNI space. Twenty mm radius spheres were generated centered on each of these DLPFC coordinates in MNI space. This sphere size is larger than the sphere size often used in intrinsic functional connectivity studies and was chosen for three reasons. First, several coordinates used in the present analysis are actually average coordinates across multiple stimulation sites scattered over several centimeters (12, 14, 19) and this larger sphere size more accurately captures this distribution. Second, even when specific coordinates are targeted, the spread of TMS stimulation can be up to several centimeters with focal figure eight coils and even greater with the FDA approved Neurostar coil (20). Finally, some of the DLPFC coordinates reported in the literature (11) seemed to reside above the cortical surface (in both Talairach and MNI space), and the larger sphere size enabled robust ROIs to still be created using the published coordinates.

A single large left DLPFC region of interest was also generated designed to cover all voxels that could reasonably be considered part of the left DLPFC by combining 25 mm radius spheres centered on the coordinates for BA9, BA46, and the standard 5 cm TMS site (Figure S1C). All DLPFC ROIs were left sided (unilateral), and masked to eliminate any unsampled voxels or voxels lying outside of gray matter as defined by the standard Harvard/Oxford gray matter template in FSL thresholded at an intensity of 70.

Data Processing

fMRI data from both datasets were processed in accordance with the strategy of Fox *et al.* 2005 (21) as implemented in Van Dijk 2010 (22). In brief, functional data were preprocessed to decrease image artifacts and between-slice timing differences. Data were then spatially smoothed using a Gaussian kernel of 6 mm full-width at half-maximum and temporally filtered (0.009 Hz < f < 0.08 Hz). Next, several spurious or nonspecific sources of variance were removed by regression of the following variables: 1) six movement parameters computed by rigid body translation and rotation during preprocessing, 2) mean whole brain signal, 3) mean brain signal within the lateral ventricles, and 4) the mean signal within a deep white matter ROI. Inclusion of the first temporal derivatives of these regressors within the linear model accounted for the time-shifted versions of spurious variance.

Time courses were extracted by averaging across voxels in each seed region. For seed regions with varying voxel values (i.e. seed maps) a weighted average was used. Correlation between extracted time courses was assessed using Pearson's correlation coefficient. For statistical testing Fisher's r-to-z transform was used and either single group or paired *t*-tests were used to determine significance (two-tailed). After averaging and statistics, Fisher z values were converted back to r values using the Fisher inverse transform. Error bars on r values reflect the standard error of Fisher z values. To generate functional connectivity maps, the Pearson's correlation coefficient was computed between the seed region time course and that of all other voxels. Fisher's r-to-z transformation was used to convert correlation maps into z maps. Group effects were tested with a random effects analysis using a one sample *t*-test. For seed-based correlation maps, images were threshold at $t = 4.25$ $p < 0.0001$ uncorrected. Similarity between seed based correlation maps was assessed using a spatial correlation coefficient across voxels (23). All data processing, calculations, and thresholding were performed in volume space. For

display purposes data were mapped to the cortical surface using CARET and the PALS atlas (24). ROIs and integer-based overlaps are displayed using average fiducial mapping option in CARET while functional data are displayed using the multi-fiducial mapping option.

Relating Functional Connectivity to Previously Reported Clinical Efficacy

Three different analyses were used to relate functional connectivity of various left DLPFC TMS sites to previously reported clinical efficacy: 1) Paired comparison of functional connectivity between two TMS sites previously shown to differ in clinical efficacy, 2) correlation between functional connectivity and clinical efficacy as predicted by a previously reported equation, and 3) correlation between functional connectivity and clinical efficacy as previously reported in individual patients.

1) To explore differences in functional connectivity between pairs of TMS sites previously shown to differ in clinical efficacy, we utilized two prior studies each comparing two DLPFC stimulation sites: Herbsman *et al.* (12) and Fitzgerald *et al.* (11). Functional connectivity was compared between each effective versus less effective site using a paired *t*-test and images were thresholded at $t = 3.0$, $p < 0.005$ uncorrected. Since two of these paired maps were generated, a combined effective-ineffective map was constructed by averaging the two individual maps then masking this with a map of voxels significant in both analyses. Local maxima (peaks) in this map were determined using the FSL Cluster algorithm, threshold of t = 5 (positive or negative), minimum cluster size of 2, and one peak per cluster. Thresholds were chosen empirically to return approximately 20-30 negative peaks and 20-30 positive peaks.

2) To compute the predicted group-level clinical efficacy of different DLPFC stimulation sites we used the empirically derived equation from Herbsman *et al.* 2009 (12): HDRS drop = -.84 + (X * -0.022) + (Y * 0.012). Since this equation was derived based on Talairach coordinates (10), these coordinates were used to compute the predicted clinical efficacy. The relationship between the predicted group-level clinical efficacy and intrinsic connectivity with the subgenual was computed using Pearson's correlation coefficient (two-tailed).

3) To determine if the above correlation between clinical efficacy and subgenual connectivity held true in individual subjects, subject-specific stimulation coordinates and clinical responses (changes in Montgomery Asberg Depression Rating Scale) were taken from Paillere-Martinot 2010 (18). Only those subjects with left sided simulation ($n = 27$) were included. Ten

mm spheres were created at each of these coordinates then masked to eliminate any unsampled voxels or voxels lying outside of gray matter as defined by the standard Harvard/Oxford gray matter template in FSL thresholded at an intensity of 70. The expected relationship between clinical efficacy and intrinsic connectivity with the subgenual was confirmed using Pearson's correlation coefficient (one-tailed given the a-priori hypothesis regarding the direction of the expected correlation).

Connectivity Based Targeting

Given the results of the above analyses, coordinates were identified in the left DLPFC that could potentially serve as optimized TMS targets by computing seed-based functional connectivity with two regions: our a priori ROI in the subgenual and our effective-ineffective map.

For the subgenual ROI functional connectivity map, local maxima (peaks) were determined using the FSL Cluster algorithm. Negative peaks were identified using a threshold of t = 10, minimum cluster size of 2, and one peak per cluster. Positive peaks were identified using a threshold of t = 8, minimum cluster size 2, and one peak per cluster except for the singe large cluster centered around the subgenual seed region for which an additional 10 peaks were included. Thresholds for peak identification were chosen empirically and were varied in order to return approximately 20-30 negative peaks and 20-30 positive peaks.

In order to use the result of our paired effective-ineffective analysis as a "seed map" for identifying optimized left DLPFC coordinates, voxels in the left DLPFC ROI were excluded and the map was inverted (multiplied by negative 1) to maintain consistency with the direction of the relationships observed with the subgenual seed (i.e. negative correlation = improved clinical efficacy). We will refer to this map as the "efficacy-based seed map." Note that the use of this seed map will bias any coordinates outside the DLPFC so additional peaks in this functional connectivity map are not reported.

Replication in Patients with Depression

To confirm that the above relationship between reported clinical efficacy and subgenual functional connectivity identified in normal subjects held true in patients with depression, we replicated our primary findings in 13 patients with major depression. Given that we were

confirming a priori hypotheses, one -tailed *t*-tests were used. These analyses were also performed in 11 normal subjects from the same dataset and compared to the 13 patients with depression using two-tailed *t*-tests.

Table S1. Peak Coordinates from Functional Connectivity Maps. Region names are displayed in the left column, local maxima for regions showing a difference in functional connectivity between effective versus ineffective DLPFC transcranial magnetic stimulation sites (see Figure S2) are shown in the middle column, and local maxima for regions showing significant functional connectivity with the subgenual cingulate (see Figure 3A) are shown in the right column. Note that both lists are divided into positive and negative peaks, although with the order reversed between lists to better illustrate commonalities. All coordinates are in MNI space (MNIx, MNIy, MNIz).

Region	**Effective-Ineffective Peaks**	**Subgenual fcMRI Peaks**
	Negative Peaks	**Positive Peaks**
Subgenual Cingulate Cortex	(-8 24 -16)	(2 16 -10)
Medial Prefrontal Cortex	(-2 52 -12) (-4 30 -22)	(-6 34 -10) (10 36 -12) (-2 44 -24) (0 60 -20)
Superior Frontal Gyrus	(-38 14 54) (22 34 48) (-4 46 36)	(-6 48 48) (18 36 54)
Middle Frontal Gyrus (BA44)	(-46 14 48)	
Posterior Cingulate/ Precuneus	(-2 -56 24) (-4 -36 36) (-2 -58 44)	(8 -52 22)
Hippocampus/PHG	(-24 -36 -20) (24 -22 -24) (-14 -32 -10)	(24 -20 -24) (-26 -20 -24)
Lateral Parietal/Occipital	(-42 -68 36) (46 -64 30)	(-40 -76 46) (54 -66 32) (-52 -70 36)
Cerebellar Tonsils	(6 -54 -48)	(-4 -50 -46)
Cerebellar Hemisphere	(42 -72 -34) (16 -88 -38) (38 -72 48) (16 -72 -26) (8 -88 -38)	
Middle Temporal Gyrus	(-58 -16 -22) (58 -4 -26)	(58 -8 -22) (-54 -10 -22)
Inferior Temporal Gyrus		(-46 -2 -44) (40 -12 -42)
Somatomotor Cortex	(-6 -32 66) (34 -24 60) (12 -28 64) (-30 -24 60)	
Orbitofrontal Cortex		(22 20 -22) (-24 18 -24)
Temporal Pole		(40 16 -46)
Frontal Pole	(-8 66 18) (-12 60 10)	(-2 58 4)
	Positive Peaks	**Negative Peaks**
DLPFC	(-38 40 32)	(-44 38 34) (40 42 30) (50 48 20)
Anterior Insula	(42 14 -6) (-42 8 -46) (-30 24 2)	(-26 18 2) (30 20 10) (34 4 12)
Operculum		(-48 10 8) (34 2 2)
Mid/Posterior Cingulate	(12 -30 42) (-10 -28 42) (8 -28 24) (-12 -38 44)	
Precuneus	(14 -70 42)	
Dorsal Anterior Cingulate/pSMA	(4 18 34)	(8 16 46)

Thalamus (mediodorsal nucleus)	(10 -22 4) (6 -16 0)	(-18 -6 12) (10 -12 0) (-22 -22 12)
Putamen	(-28 -10 6) (20 -6 14)	
Parietal Cortex BA40	(62 -34 36) (-66 -30 30)	(-42 -44 44) (36 -48 50)
Lateral Occipital Cortex BA19		(-24 -70 26)
Orbitofrontal	(-26 38 -12) (16 8 -24) (22 42 -12) (-20 6 -24)	(-46 44 2) (-46 46 16)
Right Precentral Gyrus	(54 4 34)	
Cerebellum		(-26 -72 -20)

BA, Brodmann area; DLPFC, dorsal lateral prefrontal cortex; fcMRI, functional connectivity magnetic resonance imaging; MNI, Montreal Neurological Institute; PHG, parahippocampal gyrus; pSMA, pre-supplementary motor area.

Table S2. Neuroimaging changes in the subgenual cingulate (SG) or adjacent medial prefrontal cortex (MPF) in response to dorsal lateral prefrontal cortex transcranial magnetic stimulation (TMS). Studies varied in their study population (normal controls versus depression patients), repeated TMS frequency (high or low), hemisphere (right or left), session (during a single session or after repeated sessions), and neuroimaging technique: single photon emission tomography (SPECT), positron emission tomography (PET), functional magnetic resonance imaging (fMRI), and low-resolution electromagnetic tomography (LORETA). The outcome of each study specifically in the subgenual cingulate or adjacent medial prefrontal cortex is shown. Note that many studies showed additional changes not reported in this table.

Population	Frequency	Side	Sessions	Modality	Outcome	Reference
Normal	High	Left	Single	SPECT	SG decrease	(25)
Normal	Low	Left	Single	PET	SG decrease	(26)
Depression	High	Left	Repeated	LORETA	SG decrease	(27)
Depression	Low	Right	Repeated	SPECT	SG decrease	(7)
Depression	Low	Right	Repeated	SPECT	SG decrease	(8)
Normal	High	Left	Single	PET	MPF decrease	(16)
Normal	Low	Left	Single	fMRI	MPF decrease	(28)
Depression	High	Left	Repeated	SPECT	MPF decrease	(29)
Normal	Low	Left	Single	fMRI	No change	(30)
Normal	Low	Left	Repeated	PET	No change	(33)
Normal	Low	Right	Single	PET	No change	(31)
Normal	Low or High	Left or Right	Single	PET	No change	(32)
Depression	Low	Left	Repeated	PET	No change	(34)
Depression	High	Left	Repeated	PET	MPF increase	(34)

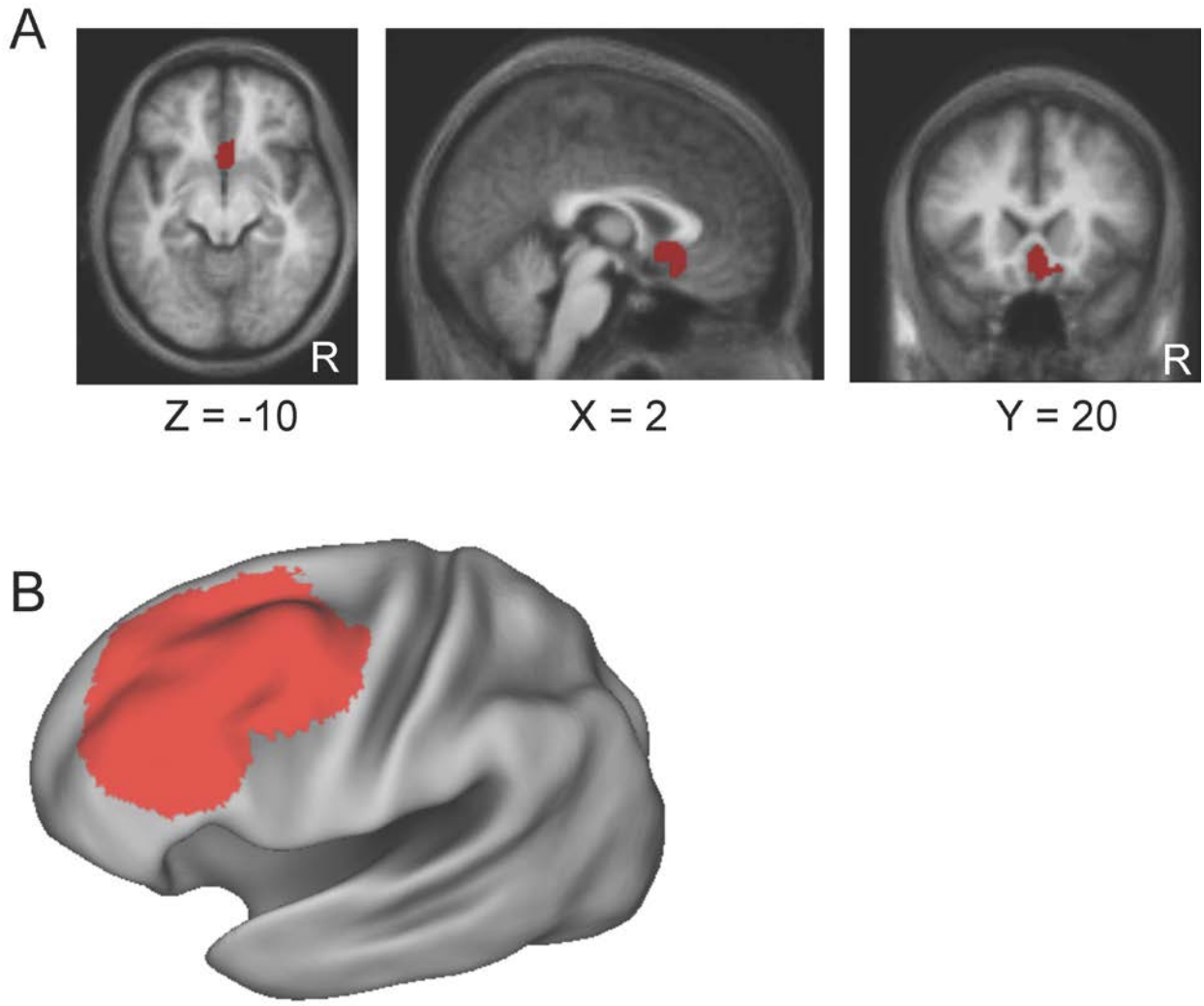

Figure S1. A priori defined regions of interest (ROI) not otherwise shown in the primary figures. **(A)** The ROI in the subgenual cingulate cortex is displayed in volume space. **(B)** The large ROI designed to cover the entire left dorsal lateral prefrontal cortex and used as a template for some analyses is shown on a lateral/oblique view of the left hemisphere. R, right.

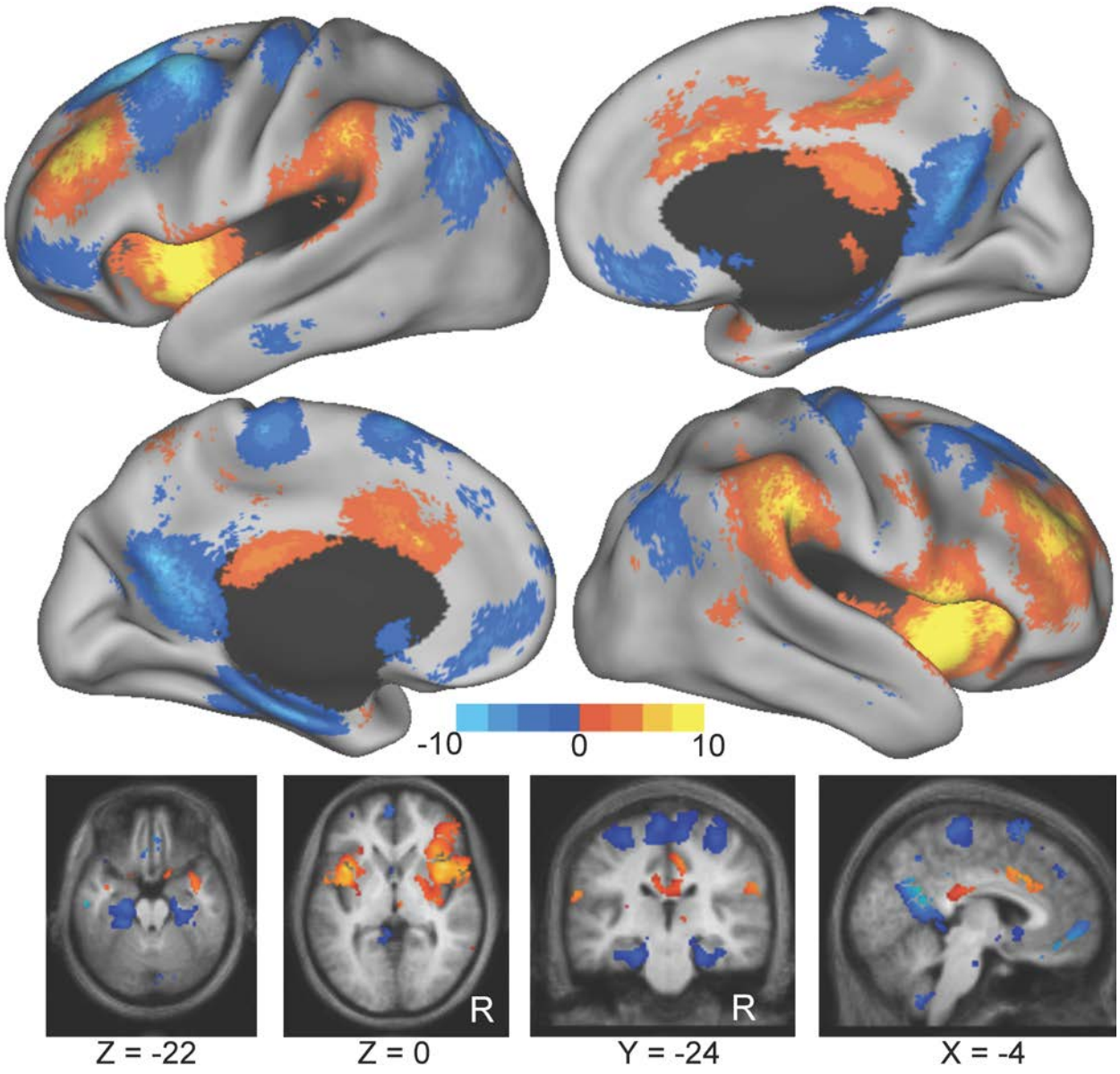

Figure S2. Differences in resting state functional connectivity between more effective versus less effective dorsal lateral prefrontal cortex (DLPFC) stimulation sites, convergence of results across both comparisons. Shown are those voxels significantly more correlated with more effective versus less effective DLPFC transcranial magnetic stimulation targets across both the Herbsman *et al.* 2009 (12) (see Figure 2B) and Fitzgerald *et al.* 2009 (11) (see Figure 2D) comparisons. Results are displayed both in surface space and in volume space. R, right.

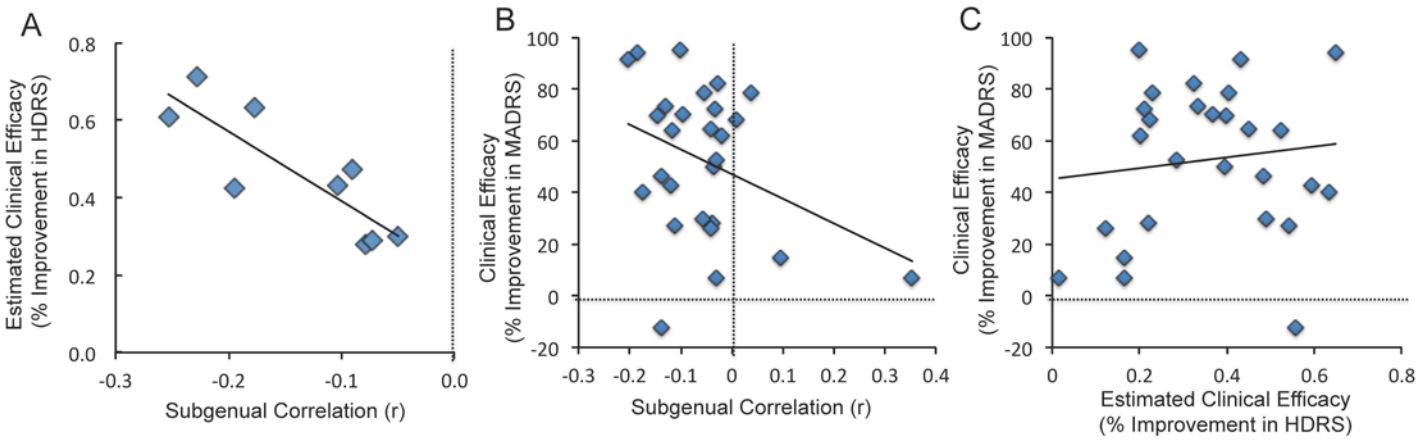

Figure S3. Relationship between reported clinical efficacy of different dorsal lateral prefrontal cortex (DLPFC) stimulation sites and functional connectivity with the subgenual cingulate. **(A)** Relationship between estimated equation-based clinical efficacy of different DLPFC stimulation sites and functional connectivity with the subgenual cingulate. For each DLPFC transcranial magnetic stimulation target reported in the literature (see Table 2) we plotted the estimated clinical efficacy (per the empirically derived equation from Herbsman *et al.* 2009 (12)) versus the resting state correlation with the subgenual cingulate. More effective targets are more negatively correlated with the subgenual cingulate (r = -0.842, p < 0.001 two-tailed). **(B)** Replication of the relationship between clinical efficacy and functional connectivity with the subgenual cingulate for left DLPFC stimulation sites in individual patients and individual's antidepressant responses. For each patient-specific left DLPFC stimulation site in the study by Paillère Martinot *et al.* (18), we plotted the reported clinical efficacy in that subject (change in the Montgomery Asberg Depression Rating Scale) versus functional connectivity between that stimulation site and the subgenual. Again, more effective targets were more negatively correlated with the subgenual (r = -0.355, p < 0.05 one-tailed). **(C)** Lack of relationship between estimated clinical efficacy (per the Herbsman equation) and measured clinical efficacy in individual patients (using the Martinot dataset). For each patient-specific left DLPFC stimulation site in the study by Paillère Martinot *et al.* (18), we plotted the reported clinical efficacy in that subject versus the estimated clinical efficacy as predicted by the Herbsman equation. Unlike the significant relationship with subgenual functional connectivity, there was no significant relationship between these variables suggesting that subgenual functional connectivity may capture variance not captured by the Herbsman equation (r = 0.122, p > 0.25 one-tailed). HDRS, Hamilton Depression Rating Scale; MADRS, Montgomery Asberg Depression Rating Scale.

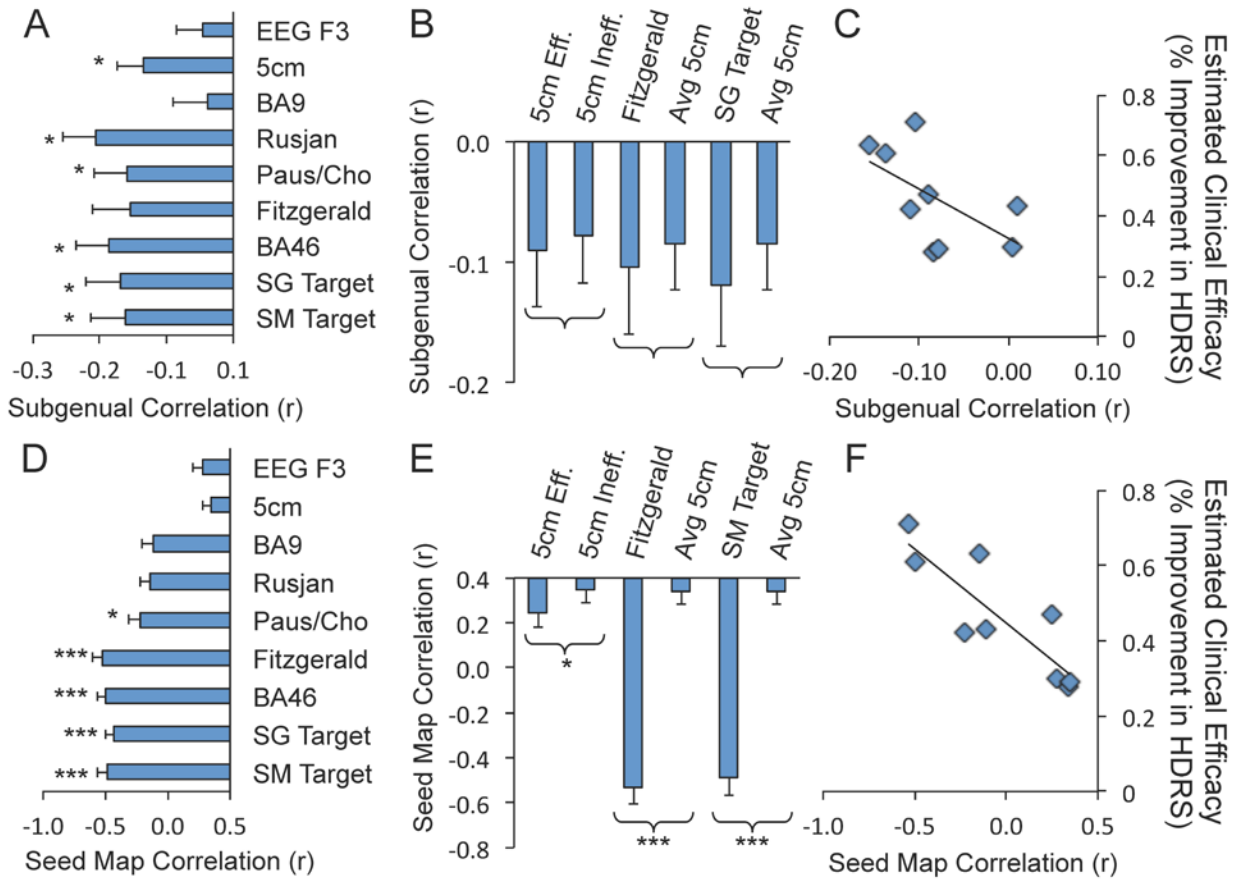

Figure S4. Replication of principal findings in 11 control subjects from the same dataset as the 13 depressed patients. Time course correlations are shown between regions of interest (ROIs) in the dorsal lateral prefrontal cortex (DLPFC) and the subgenual seed region (**A-C**) or the efficacy-based seed map (**D-F**). There is an anticorrelation between transcranial magnetic stimulation targets in the DLPFC and the subgenual (**A**). Paired comparisons show a trend towards stronger anticorrelation with more effective sites (**B**). The relationship between estimated clinical efficacy (using the Herbsman equation) and anticorrelation with the subgenual is similar to that previously observed (**C**; $r^2 = 0.34$, $p = 0.051$). Using the efficacy-based seed map rather than the small subgenual seed region produces similar but more significant results including examination of regional time course correlations (**D**), paired comparisons (**E**), and the correlation between functional connectivity and estimated clinical efficacy (**F**; $r^2 = 0.73$, $p < 0.005$). Labels for DLPFC ROIs are as in Figures 1 and 2 with the addition of optimized DLPFC targets identified in normal subjects using the subgenual seed region (SG Target) and the efficacy-based seed map

(SM Target). $*p < 0.05$, $**p < 0.001$, $***p < 10^{-4}$. Overall, this small population of 11 subjects shows the same pattern of results seen in both our original population of 98 normal subjects and the 13 subjects with depression. There are no significant differences between these 11 normal subjects and the 13 subjects with depression from the same dataset. BA, Brodmann area; HDRS, Hamilton Depression Rating Scale.

Supplemental References

1. Yeo BT, Krienen FM, Sepulcre J, Sabuncu MR, Lashkari D, Hollinshead M, *et al*. (2011): The organization of the human cerebral cortex estimated by functional connectivity. *J Neurophysiol.* 106:1125-65.
2. van der Kouwe AJ, Benner T, Salat DH, Fischl B (2008): Brain morphometry with multiecho MPRAGE. *Neuroimage*. 40:559-569.
3. Wu J, Buchsbaum MS, Gillin JC, Tang C, Cadwell S, Wiegand M, *et al*. (1999): Prediction of antidepressant effects of sleep deprivation by metabolic rates in the ventral anterior cingulate and medial prefrontal cortex. *Am J Psychiatry*. 156:1149-1158.
4. Mayberg HS, Brannan SK, Tekell JL, Silva JA, Mahurin RK, McGinnis S, *et al*. (2000): Regional metabolic effects of fluoxetine in major depression: serial changes and relationship to clinical response. *Biol Psychiatry*. 48:830-843.
5. Drevets WC, Bogers W, Raichle ME (2002): Functional anatomical correlates of antidepressant drug treatment assessed using PET measures of regional glucose metabolism. *Eur Neuropsychopharmacol*. 12:527-544.
6. Mayberg HS, Lozano AM, Voon V, McNeely HE, Seminowicz D, Hamani C, *et al*. (2005): Deep brain stimulation for treatment-resistant depression. *Neuron*. 45:651-660.
7. Kito S, Fujita K, Koga Y (2008): Regional cerebral blood flow changes after low-frequency transcranial magnetic stimulation of the right dorsolateral prefrontal cortex in treatment-resistant depression. *Neuropsychobiology*. 58:29-36.
8. Kito S, Hasegawa T, Koga Y (2011): Neuroanatomical correlates of therapeutic efficacy of low-frequency right prefrontal transcranial magnetic stimulation in treatment-resistant depression. *Psychiatry Clin Neurosci*. 65:175-182.
9. Nahas Z, Teneback C, Chae JH, Mu Q, Molnar C, Kozel FA, *et al*. (2007): Serial vagus nerve stimulation functional MRI in treatment-resistant depression. *Neuropsychopharmacology*. 32:1649-1660.
10. Talairach J, Tournoux P (1988): *Co-Planar Stereotaxic Atlas of the Human Brain*. New York: Thieme Medical Publishers, Inc.
11. Fitzgerald PB, Hoy K, McQueen S, Maller JJ, Herring S, Segrave R, *et al*. (2009): A randomized trial of rTMS targeted with MRI based neuro-navigation in treatment-resistant depression. *Neuropsychopharmacology*. 34:1255-1262.
12. Herbsman T, Avery D, Ramsey D, Holtzheimer P, Wadjik C, Hardaway F, *et al*. (2009): More lateral and anterior prefrontal coil location is associated with better repetitive transcranial magnetic stimulation antidepressant response. *Biol Psychiatry*. 66:509-515.
13. Rusjan PM, Barr MS, Farzan F, Arenovich T, Maller JJ, Fitzgerald PB, *et al*. (2010): Optimal transcranial magnetic stimulation coil placement for targeting the dorsolateral prefrontal cortex using novel magnetic resonance image-guided neuronavigation. *Hum Brain Mapp.* 31:1643-1652.
14. Herwig U, Padberg F, Unger J, Spitzer M, Schonfeldt-Lecuona C (2001): Transcranial magnetic stimulation in therapy studies: examination of the reliability of "standard" coil positioning by neuronavigation. *Biol Psychiatry*. 50:58-61.
15. Cho SS, Strafella AP (2009): rTMS of the left dorsolateral prefrontal cortex modulates dopamine release in the ipsilateral anterior cingulate cortex and orbitofrontal cortex. *PloS one*. 4:e6725.

16. Paus T, Castro-Alamancos Ma, Petrides M (2001): Cortico-cortical connectivity of the human mid-dorsolateral frontal cortex and its modulation by repetitive transcranial magnetic stimulation. *Eur J Neurosci.* 14:1405-1411.
17. Rajkowska G, Goldman-Rakic PS (1995): Cytoarchitectonic definition of prefrontal areas in the normal human cortex: II. Variability in locations of areas 9 and 46 and relationship to the Talairach Coordinate System. *Cereb Cortex*. 5:323-337.
18. Paillère Martinot M-L, Galinowski A, Ringuenet D, Gallarda T, Lefaucheur J-P, Bellivier F, *et al*. (2010): Influence of prefrontal target region on the efficacy of repetitive transcranial magnetic stimulation in patients with medication-resistant depression: a [(18)F]-fluorodeoxyglucose PET and MRI study. *Int J Neuropsychopharmacol.*. 13:45-59.
19. Herwig U, Satrapi P, Schonfeldt-Lecuona C (2003): Using the international 10-20 EEG system for positioning of transcranial magnetic stimulation. *Brain Topogr*. 16:95-99.
20. Wagner T, Valero-Cabre A, Pascual-Leone A (2007): Noninvasive human brain stimulation. *Annu Rev Biomed Eng.* 9:527-565.
21. Fox MD, Snyder AZ, Vincent JL, Corbetta M, Van Essen DC, Raichle ME (2005): The human brain is intrinsically organized into dynamic, anticorrelated functional networks. *PNAS*. 102:9673-9678.
22. Van Dijk KR, Hedden T, Venkataraman A, Evans KC, Lazar SW, Buckner RL (2010): Intrinsic functional connectivity as a tool for human connectomics: theory, properties, and optimization. *J Neurophysiol.* 103:297-321.
23. Fox MD, Corbetta M, Snyder AZ, Vincent JL, Raichle ME (2006): Spontaneous neuronal activity distinguishes human dorsal and ventral attention systems. *PNAS*. 103:10046-10051.
24. Van Essen DC (2005): A population-average, landmark- and surface-based (PALS) atlas of human cerebral cortex. *Neuroimage*. 28:635-662.
25. George MS, Stallings LE, Speer AM, Nahas Z, Spicer KM, Vincent DJ, *et al*. (1999): Prefrontal repetitive transcranial magnetic stimulation (rTMS) changes relative perfusion locally and remotely. *Hum Psychopharmacol.* 14:161-170.
26. Kimbrell Ta, Dunn RT, George MS, Danielson AL, Willis MW, Repella JD, *et al*. (2002): Left prefrontal-repetitive transcranial magnetic stimulation (rTMS) and regional cerebral glucose metabolism in normal volunteers. *Psychiatry Res.* 115:101-113.
27. Narushima K, McCormick LM, Yamada T, Thatcher RW, Robinson RG (2010): Subgenual cingulate theta activity predicts treatment response of repetitive transcranial magnetic stimulation in participants with vascular depression. *J Neuropsychiatry Clin Neurosci.* 22:75-84.
28. Li X, Nahas Z, Kozel FA, Anderson B, Bohning DE, George MS (2004): Acute left prefrontal transcranial magnetic stimulation in depressed patients is associated with immediately increased activity in prefrontal cortical as well as subcortical regions. *Biol Psychiatry*. 55:882-890.
29. Teneback CC, Nahas Z, Speer AM, Molloy M, Stallings LE, Spicer KM, *et al*. (1999): Changes in prefrontal cortex and paralimbic activity in depression following two weeks of daily left prefrontal TMS. *J Neuropsychiatry Clin Neurosci.* 11:426.
30. Nahas Z, Lomarev M, Roberts DR, Shastri a, Lorberbaum JP, Teneback C, *et al*. (2001): Unilateral left prefrontal transcranial magnetic stimulation (TMS) produces intensity-dependent bilateral effects as measured by interleaved BOLD fMRI. *Biol Psychiatry*. 50:712-720.

31. Eisenegger C, Treyer V, Fehr E, Knoch D (2008): Time-course of "off-line" prefrontal rTMS effects--a PET study. *Neuroimage*. 42:379-384.
32. Knoch D, Treyer V, Regard M, Muri RM, Buck A, Weber B (2006): Lateralized and frequency-dependent effects of prefrontal rTMS on regional cerebral blood flow. *Neuroimage*. 31:641-648.
33. Speer AM, Willis MW, Herscovitch P, Daube-Witherspoon M, Shelton JR, Benson BE, *et al*. (2003): Intensity-dependent regional cerebral blood flow during 1-Hz repetitive transcranial magnetic stimulation (rTMS) in healthy volunteers studied with H215O positron emission tomography: II. Effects of prefrontal cortex rTMS. *Biol Psychiatry*. 54:826-832.
34. Speer aM, Kimbrell Ta, Wassermann EM, D Repella J, Willis MW, Herscovitch P, *et al*. (2000): Opposite effects of high and low frequency rTMS on regional brain activity in depressed patients. *Biol Psychiatry*. 48:1133-1141.